Lecture 7:
X-Ray techniques and microscopies

- Miller indices
- Powder X-Ray Diffraction (XRD)
  - Powder pattern databases
  - Phase idenfication with powder XRD
- Thin film X-Ray techniques
  - Grazing incidence XRD
  - X-Ray Reflection (XRR)
- Microscopic methods
  - Scanning Electron Microscopy (SEM)
  - Transmission Electron Microscopy (TEM)

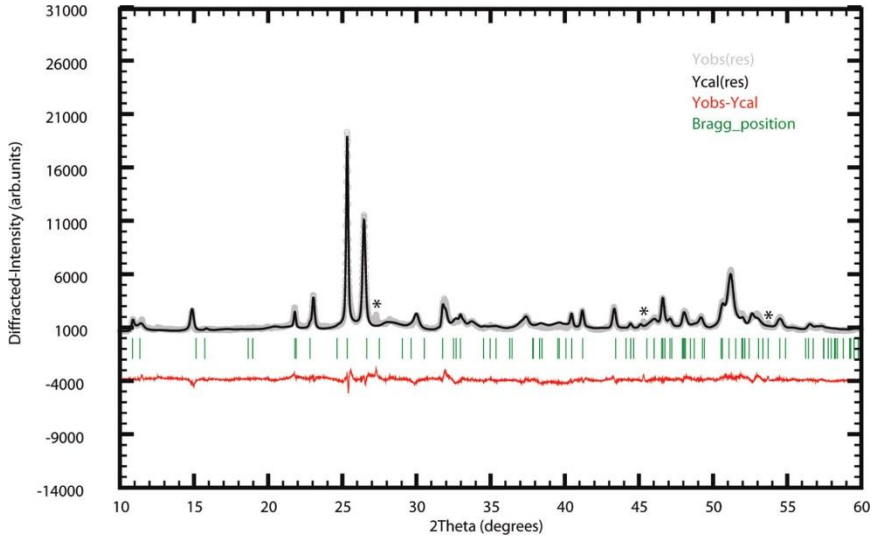

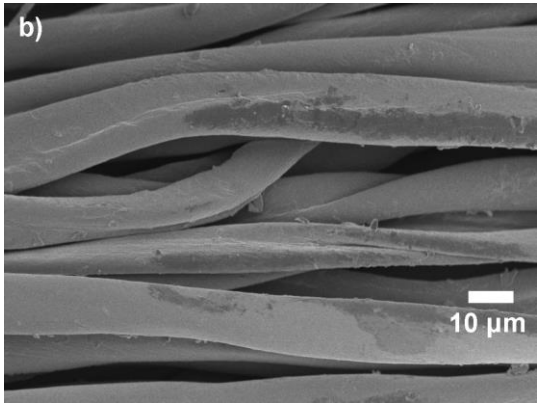

Figures: AJK

Structure of crystalline solids

1. Local structure / Defects

Spectroscopy
- IR, Raman
- NMR, ESR
- X-Ray spectroscopies
- Electron spectroscopies

2. Unit cell (average crystal structure)

Diffraction techniques
- X-Ray diffraction (XRD)
- Neutron diffraction
- Electron diffraction

3. Nanostructure

Microscopy and diffraction
- Transmission electron microscopy
- Scanning electron microscopy
- X-Ray diffraction (particle size)
- Pair distribution function analysis

4. Microstructure (grains, grain boundaries, surfaces)

- Scanning electron microscopy
- X-Ray diffraction (particle size)
- X-Ray tomography
- Elemental analysis

Ref: West p. 230

Miller indices (1)

See also Solid State Chemistry Wiki

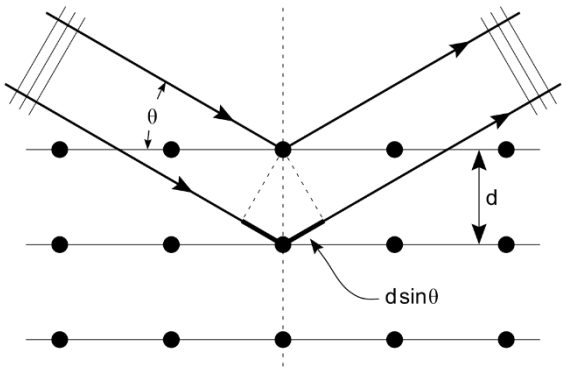

Figure: Wikipedia

- A very fundamental concept in XRD is the ***lattice plane***.
  - Introduced with Bragg's law of diffraction
  - Sometimes coincide with "atomic layers"

- Lattice planes are labelled by assigning three numbers known as ***Miller indices***
- In the figure, the origin of the unit cell is at point 0
- The figure shows two planes which are parallel and pass obliquely through the unit cell
- A third plane in this set passes through the origin
- Each of these planes continues out to the surface of the crystal and cuts through many more unit cells
- There are many more planes parallel to the two shown, but they do not pass through this particular unit cell

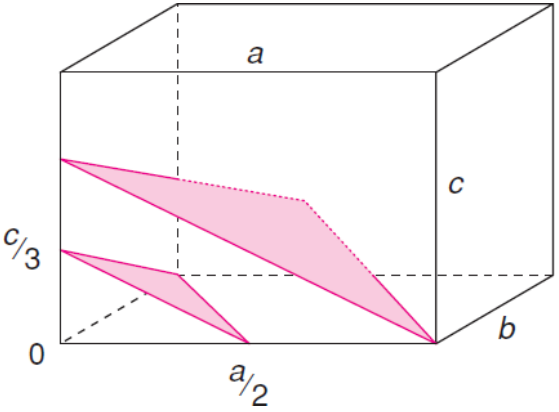

VESTA has excellent tools for the visualization of lattice planes!
See MyCourses -> Software -> VESTA documentation

Ref: West p. 16

Miller indices (2)

In order to assign Miller indices to a set of planes, there are four stages:

1. Identify the unit cell, choose the origin and label the axes *a*, *b*, *c* and angles *α* (between *b* and *c*), *β* between *a* and *c*) and *γ* (between *a* and *b*).
2. For a particular set of lattice planes, identify that plane which is adjacent to the one that passes through the origin.
3. Find the intersection of this plane on the three axes of the cell and write these intersections as fractions of the cell edges. The plane in figure cuts *x*-axis at *a*/2, *y*-axis at *b* and *z*-axis at *c*/3 -> the fractional intersections are 1/2, 1, 1/3.
4. Take reciprocals of these fractions and write the three numbers in parentheses; this gives (213). These three integers, (213), are the Miller indices of the plane and all other planes parallel to it (separated by the same *d*-spacing).

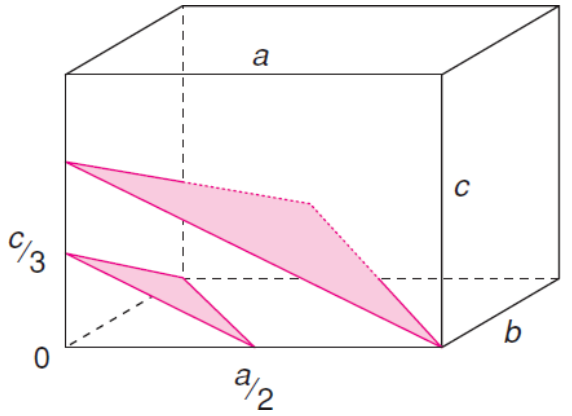

Ref: West p. 16

Miller indices (3)

- In (a), the shaded plane cuts *x*, *y* and *z* at 1*a*, ∞*b* and 1*c*, that is, the plane is parallel to *b*. Taking reciprocals of 1, ∞, and 1 gives (101) for the Miller indices
  - A Miller index of 0 means that the plane is parallel to that axis
- In (b), the planes of interest comprise opposite faces of the unit cell. We cannot determine directly the indices of plane 1 as it passes through the origin. Plane 2 has intercepts of 1*a*, ∞*b* and ∞*c* and Miller indices of (100)
- (c) has twice as many planes as in (b). To find the Miller indices, consider plane 2, which is the one that is closest to the origin but without passing through it.
  - Intercepts are 1/2, ∞ and ∞ -> the Miller indices are (200).
  - Miller index of 2 -> The plane cuts the relevant axis at half the cell edge.

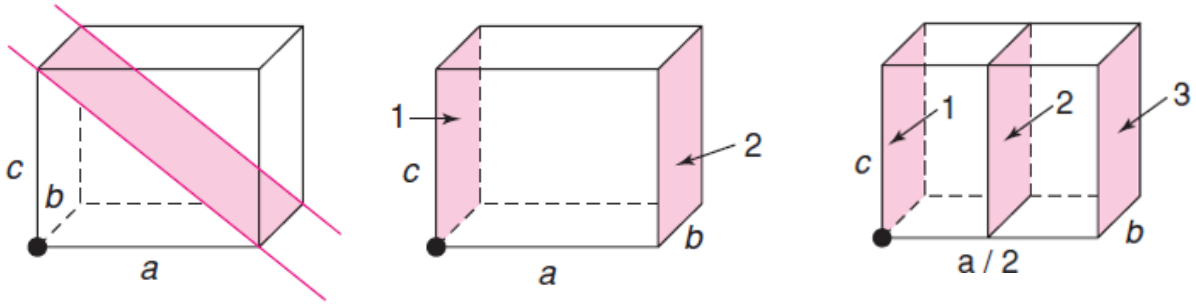

(a) (101) (b) (100) (c) (200)

Ref: West p. 16

Miller indices and directions

- The general symbol for Miller indices is (*hkl*).
- **Brackets** {} are used to indicate sets of planes that are equivalent
  - For example, the sets (100), (010), and (001) are equivalent in cubic crystals and may be represented collectively as {100}.
- **Square brackets** [] are used to denote **direction** [*hkl*]
  - For cubic systems, perpendicular to the (*hkl*) plane of the same indices
  - This is only sometimes true in non-cubic systems
- **Angle brackets** <> are used to indicate sets of directions which are equivalent
  - Directions [100], [010], and [001] are equivalent in cubic crystals and may be represented collectively as <100>.

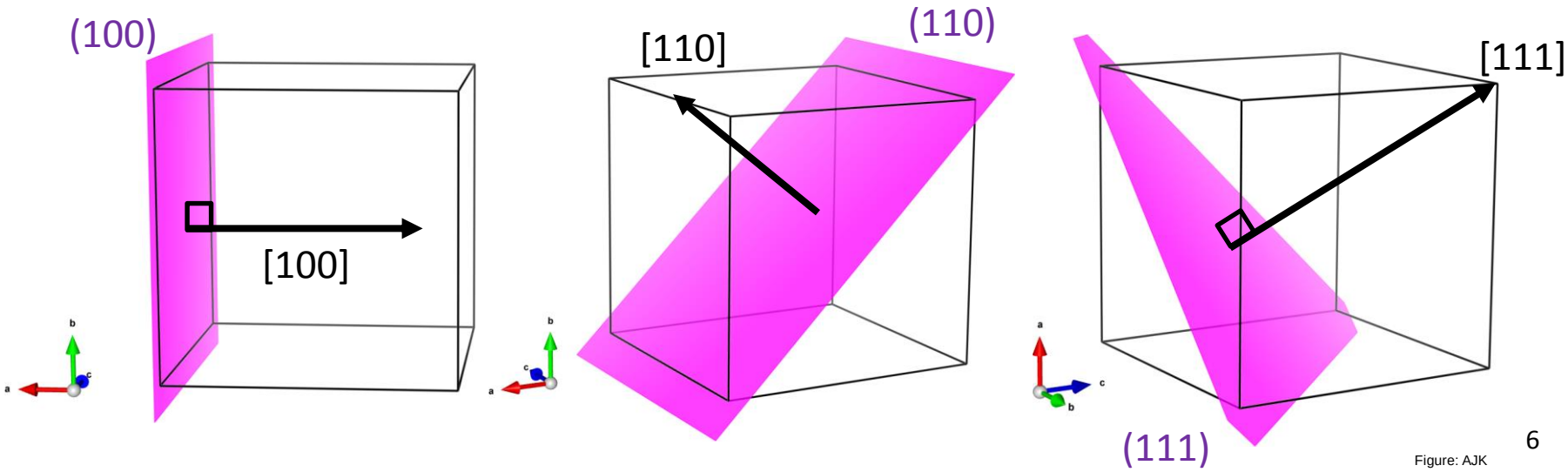

Figure: AJK

Structure determination from single-crystal and powder XRD

- X-ray diffraction has been used for over a century in two main areas
  - **Structure determination** of crystalline materials (single crystal and powder XRD)
  - **Fingerprint identification** of crystalline materials (powder XRD)
- Here the focus is on the fingerprint identification of materials *via* powder XRD
  - Structure determination is discussed in detail on the course **Crystallography Basics and Structural Characterization** (CHEM-E4205)
  - Lectured in Fall semester (Period I)

Figure: Susan Lehman / physics.wooster.edu

X-ray diffraction pattern of aluminum single crystal (left) and powder (right)

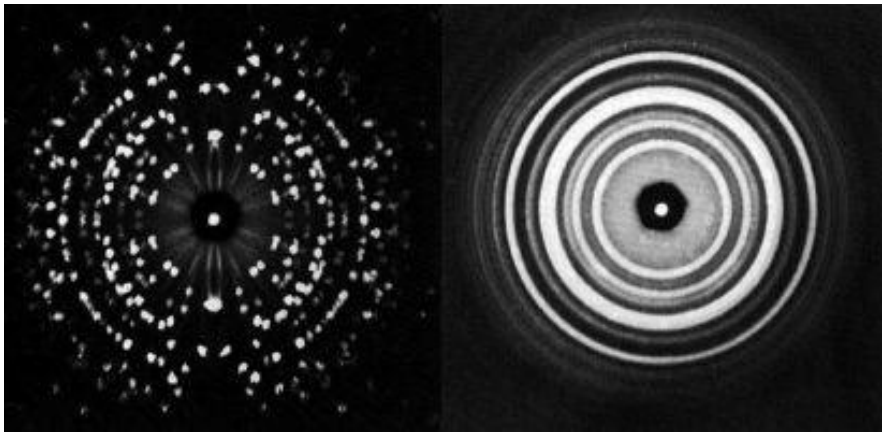

Diffractometers

- First diffractometer was built by Max von Laue in 1912
- Nowadays, numerous different types of diffractometers used for various applications
- Table-top XRD
  - Powder XRD phase identification (very useful in e.g. process control)
  - Small-molecule single-crystal XRD
- Laboratory XRD (single-crystal / powder / thin film)
  - Structures of single-crystals are rather routinely solved
  - Structures of polycrystalline powders can be solved with **Rietveld refinement**
  - Sometimes synchrotron radiation required to obtain good enough powder data

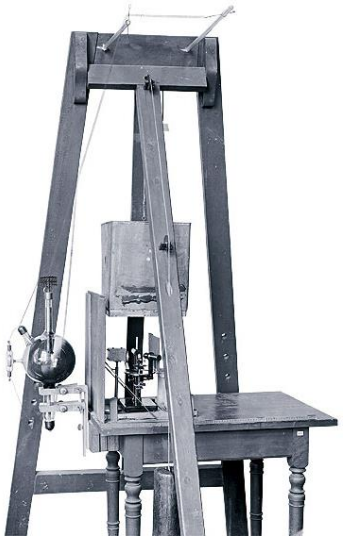

Synchrotron radiation

- Synchrotrons are particle accelerators that generate very bright X-ray beams
  - High intensity photon beam allows rapid experiments or use of weakly scattering crystals (https://en.wikipedia.org/wiki/Synchrotron_radiation)
  - High brilliance from highly collimated photon beam
- Large international facilities. For example, ESRF annual figures: budget ~100 M€, ~8000 visitors and ~2000 experiments. Particularly important for biomolecules.

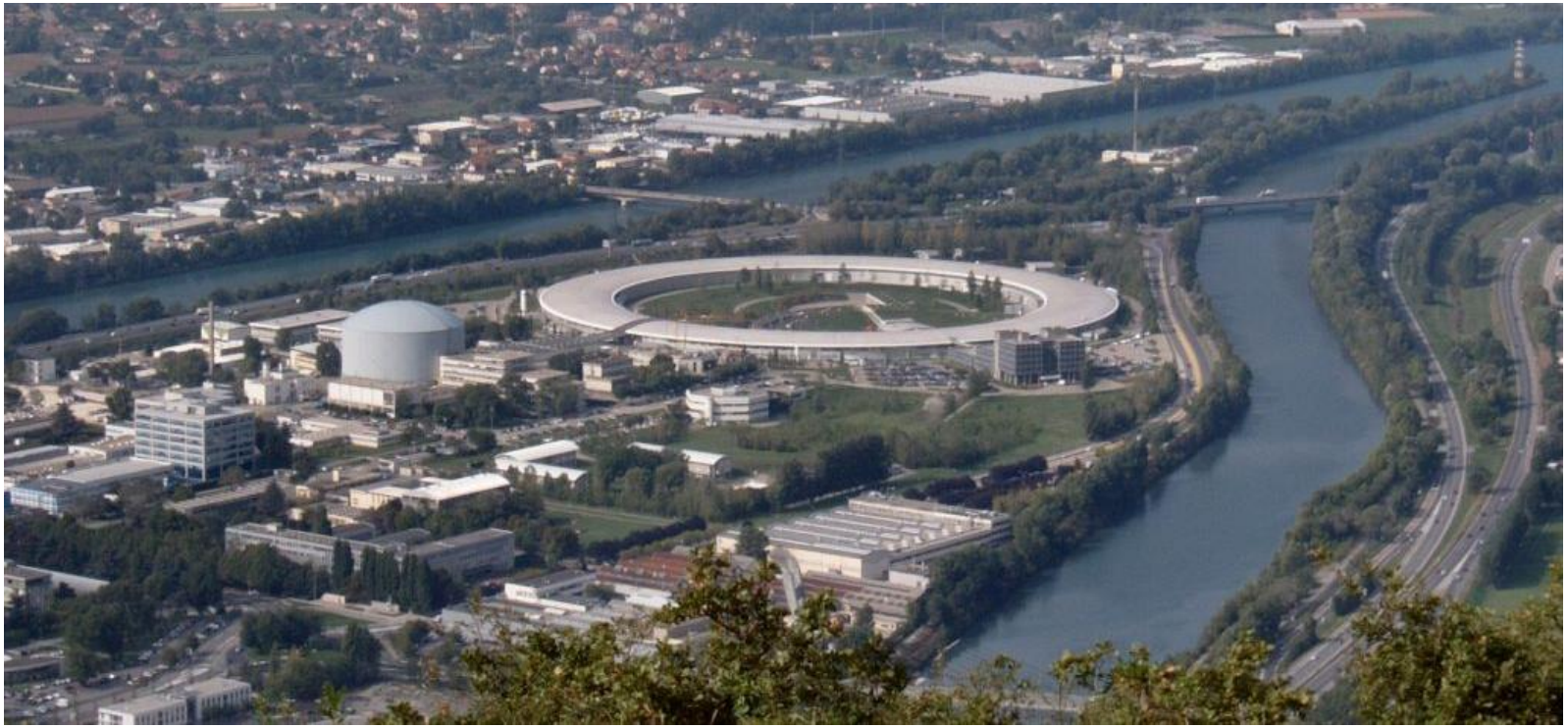

European Synchrotron Radiation Facility (ESRF) in Grenoble

Figure: Wikipedia

Structure solution from XRD

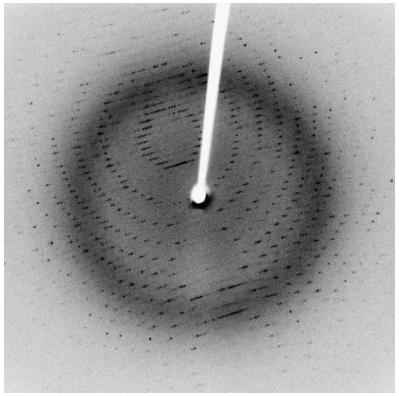

Single crystal diffraction pattern

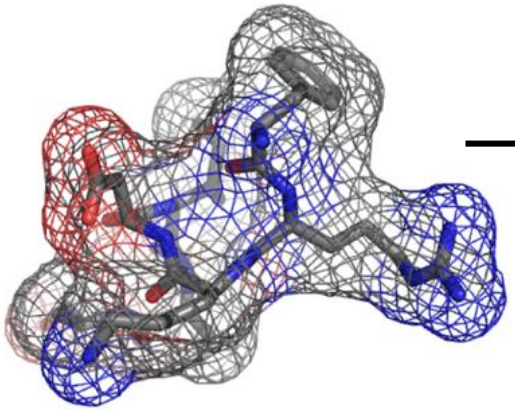

Electron density map

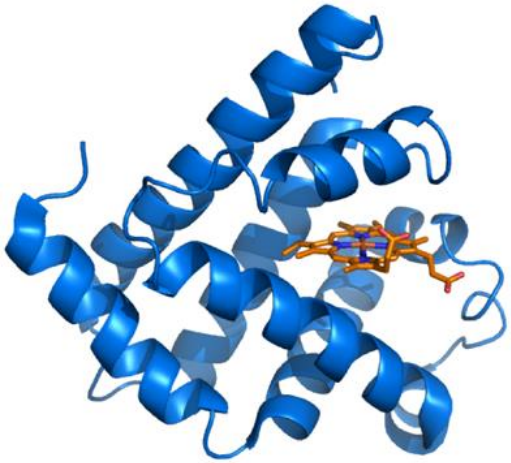

Structural model

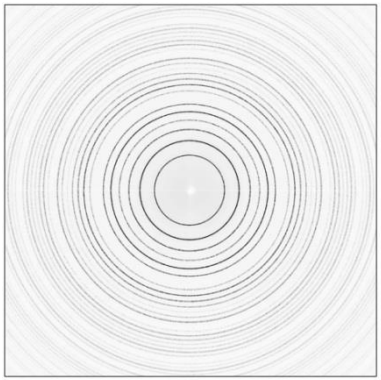

Powder diffraction pattern

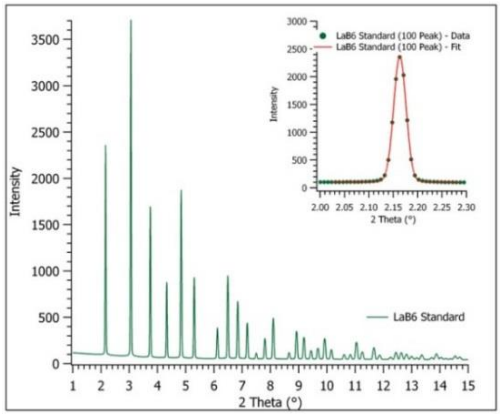

Rietveld refinement

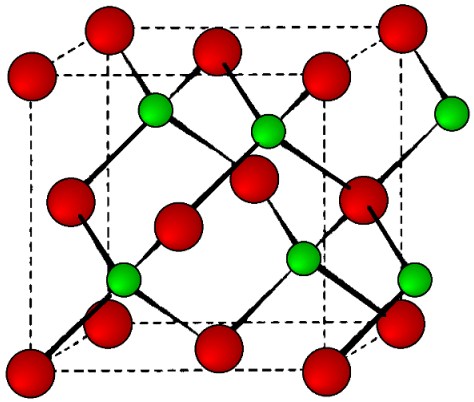

Structural model

Neutron Diffraction

- The sample is bombarded with neutrons instead of X-Rays
- Similar to synchrotron XRD, the facilities are very expensive and international collaboration is required
- Neutron beams are usually of low intensity, so large sample sizes are required (at least 1 mm^3)
- Typically polycrystalline samples
- Useful for locating light atoms, especially hydrogens (not normally possible in XRD)
- Very important application: magnetic structure of materials

Figure: John Loveday

ISIS neutron (and muon) source in Oxford, UK

Ref: West p. 266

Magnetic structure analysis

- Neutrons possess a magnetic dipole moment and interact with unpaired electrons
- Figure shows neutron diffraction investigation of antiferromagnetic MnO below and above the magnetic ordering temperature (**116 K**)

Additional reflections from **magnetic** superstructure

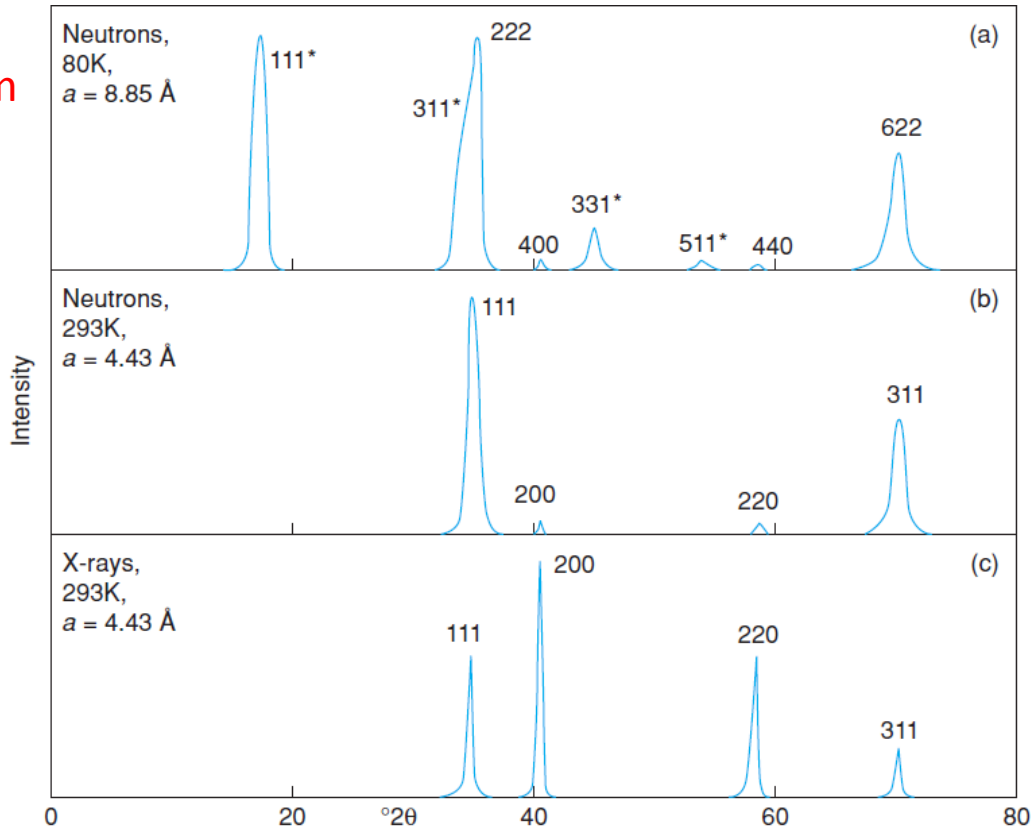

Figure 5.26 *Schematic neutron and powder XRD patterns for MnO for λ = 1.542 Å. Peaks are assigned Miller indices for the cubic unit cells given. Neutron data adapted from Shull, Strauser and Wollan,* Phys. Rev., 83, *333, © 1951 American Physical Society.*

Ref: West p. 269

Phase identification with XRD

- Powder XRD is a very powerful technique for the identification of solid phases
- Each crystalline phase has a characteristic powder XRD pattern which can be used as a fingerprint for identification purposes
  - Powder XRD patterns can be simulated if the crystal structure is known
- The two variables in a powder pattern are
  - **Peak position**, i.e. *d*-spacing, which can be measured very accurately
  - **Intensity**, which can be measured either qualitatively or quantitatively
- The normal practice in using XRD patterns for identification purposes is to pay **most attention to the *d*-spacings** and check that the intensities are roughly correct
- https://www.doitpoms.ac.uk/tlplib/xray-diffraction/powder.php
- http://www.doitpoms.ac.uk/tlplib/xray-diffraction/phase_identification.php

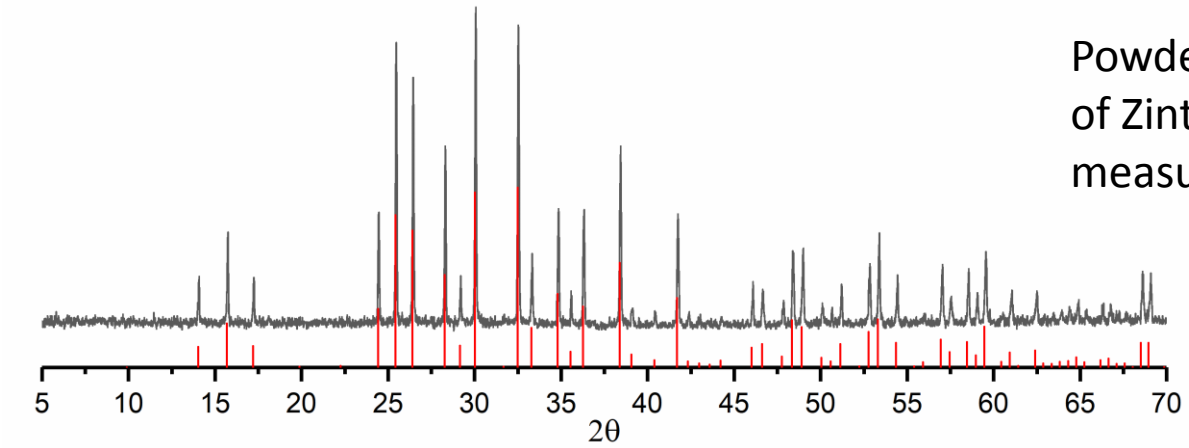

Powder X-ray diffractogram of Zintl phase K_4Si_4 (gray: measured; red: simulated).

Figure: Lorenz Schiegerl / TUM

Powder pattern matching

See Solid State Chemistry Wiki for further databases

- Powder Diffraction File (PDF)
  - 350 000+ powder patterns
  - Expensive licences, normally fixed to to a single computer
  - Pattern matching software bundled with diffractometers
- Powder pattern matching is also possible with Crystallography Open Database
  - See MyCourses -> Databases -> COD documentation
- VESTA can simulate XRD powder patterns
  - See MyCourses -> Software -> VESTA documentation

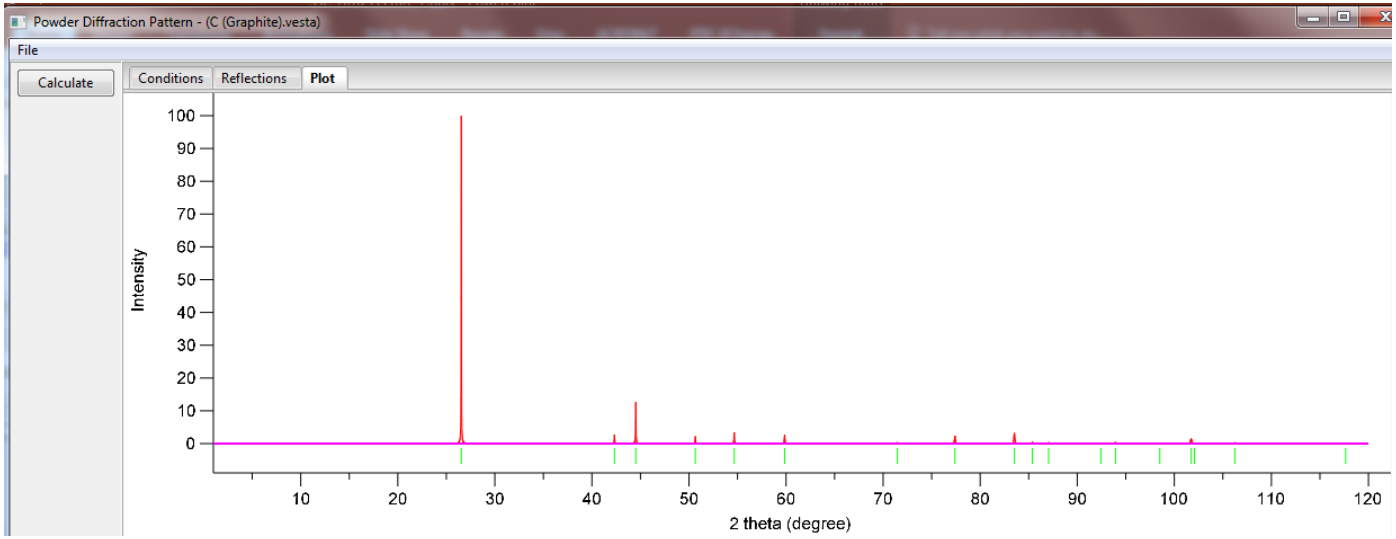

Figure: AJK

Following phase transitions with powder XRD

rhombohedral $\xrightarrow{-110°C}$ orthorhombic $\xrightarrow{28°C}$ tetragonal $\xrightarrow{125°C}$ cubic $\xrightarrow{1470°C}$ hexagonal

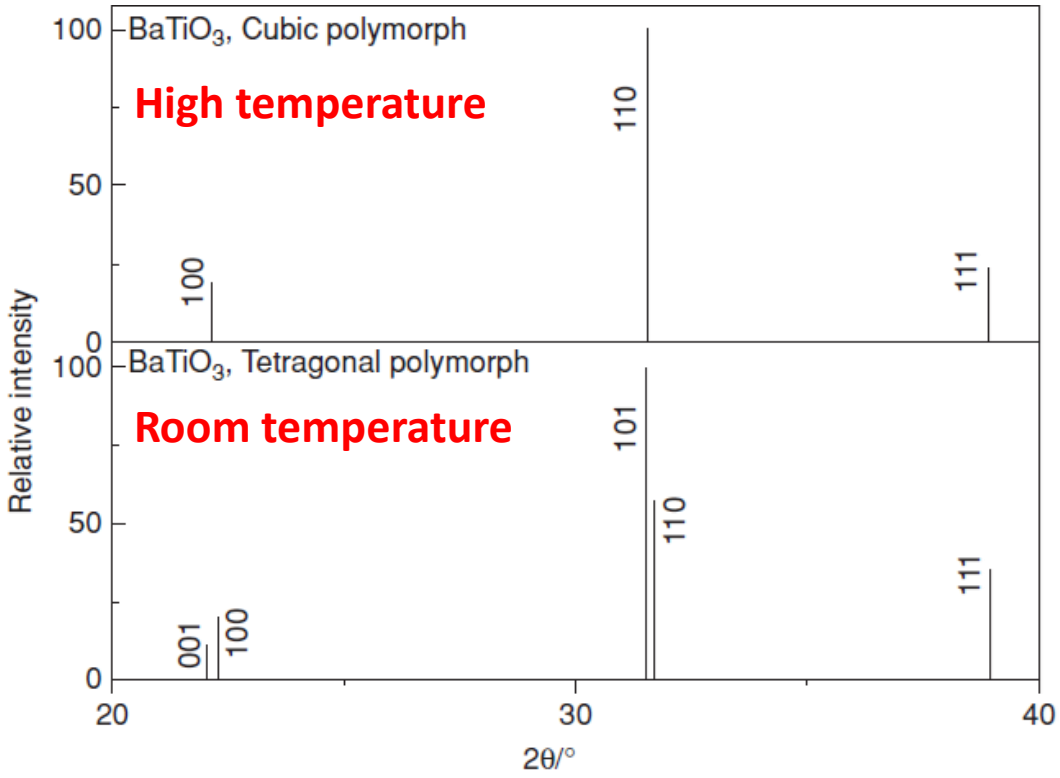

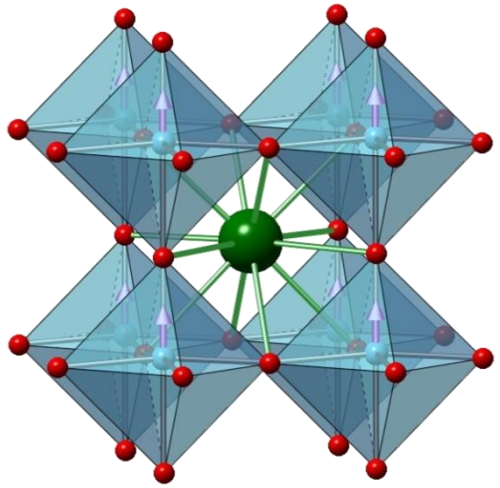

$BaTiO_3$ perovskite

Figure 5.17 *Section of the powder XRD patterns of $BaTiO_3$ showing the cubic polymorph and line splittings associated with the tetragonal polymorph. Note the difference in intensities of 001 and 100 lines and of the 101 and 110 lines of tetragonal $BaTiO_3$, which are a direct consequence of their different multiplicities. By contrast, the 111 reflection is a singlet in both cubic and tetragonal polymorphs.*

Grazing incidence X-Ray diffraction

See [Solid State Chemistry Wiki]

PANalytical

GIXRD - Thin film depth profiling phase analysis

With normal XRD, signal from substrate would dominate

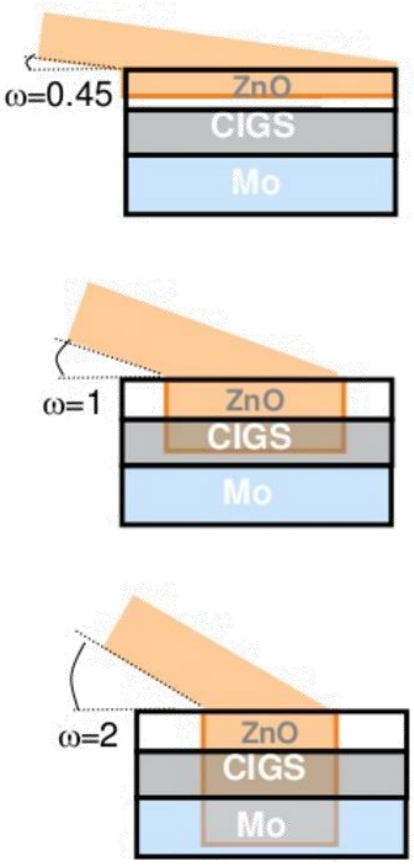

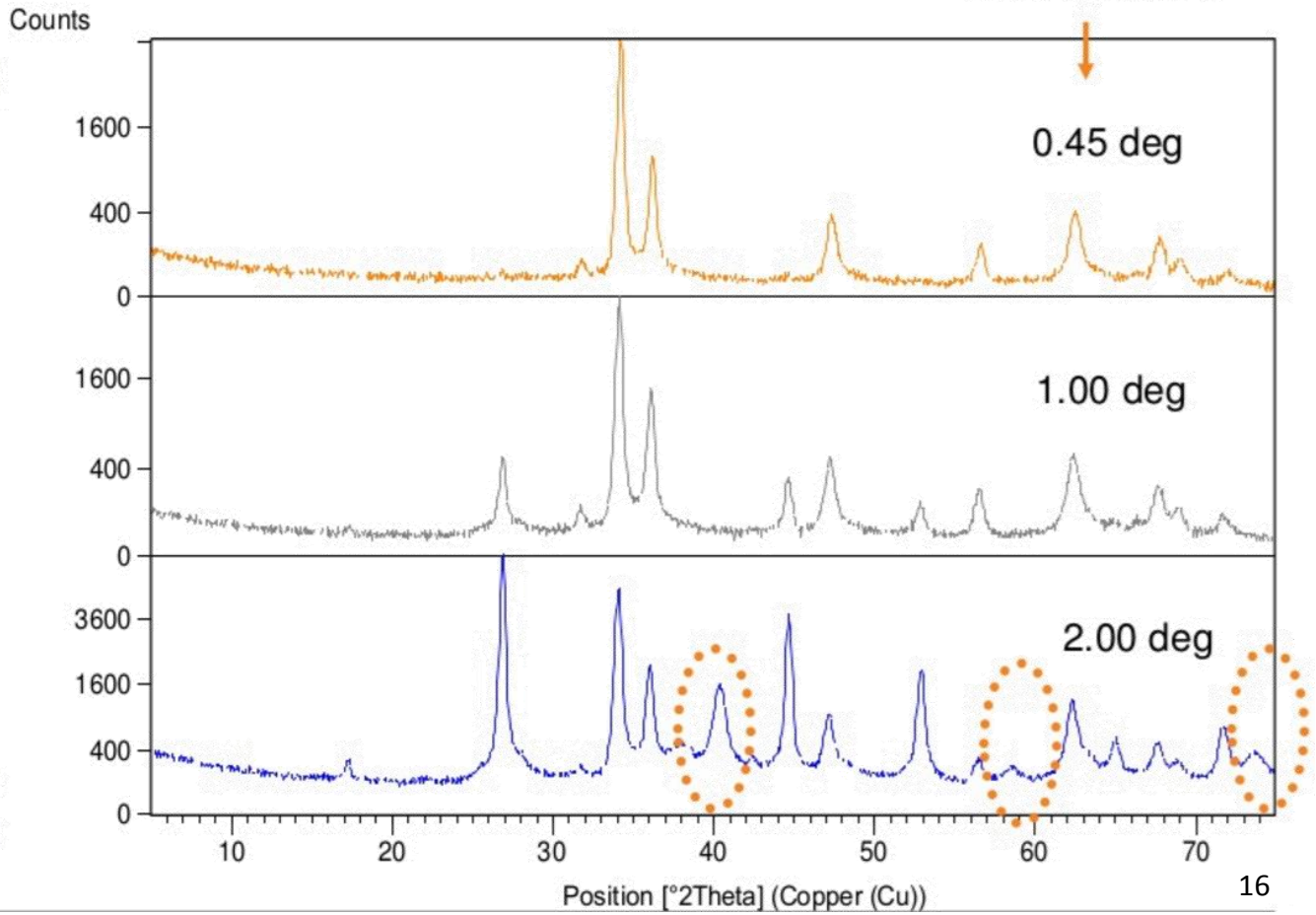

X-Ray Reflectivity (XRR) analysis for thin-film samples

Topic available at Solid State Chemistry Wiki!

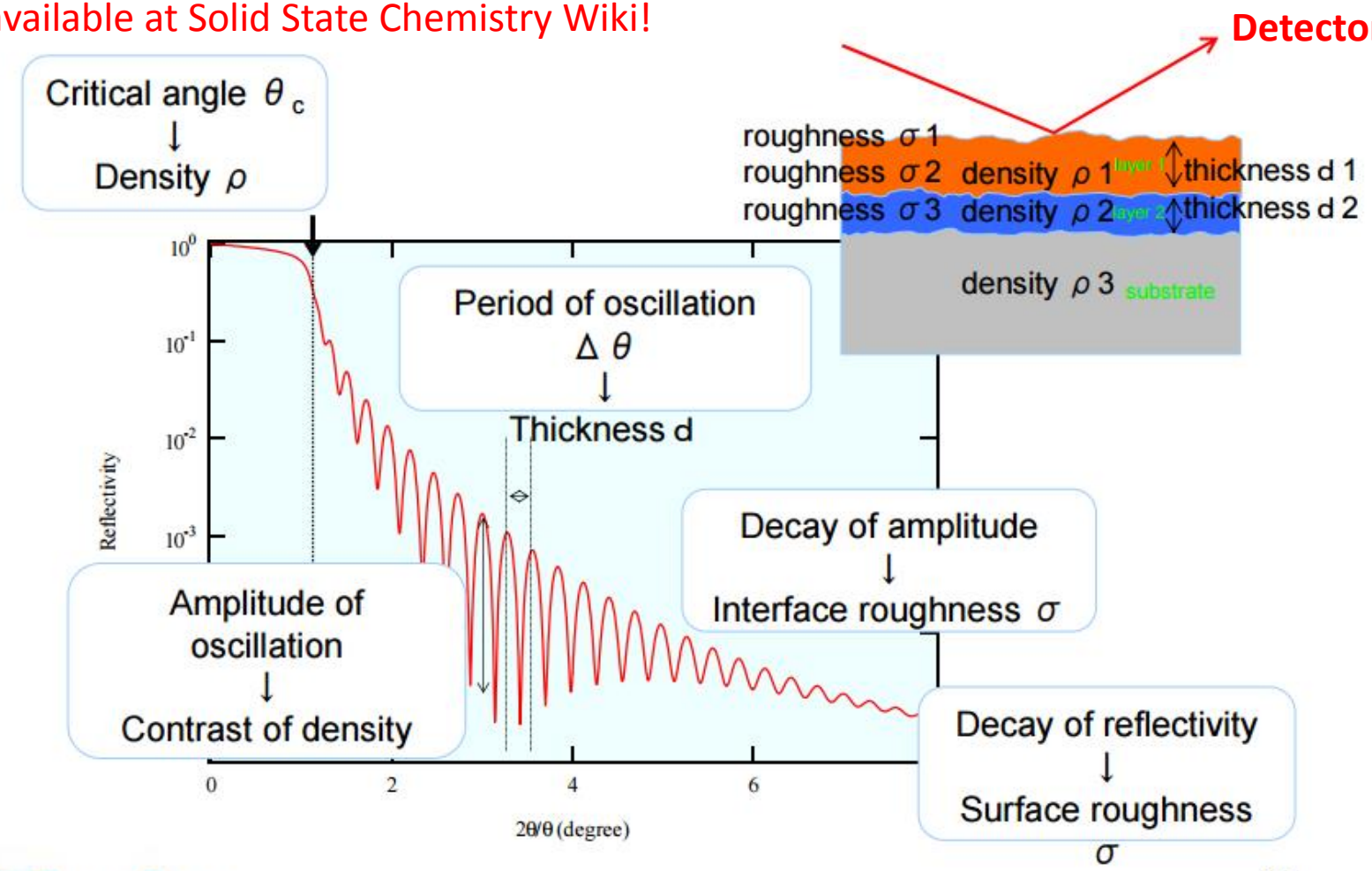

Rigaku

29

Microscopic characterization methods

- With optical microscopes, particles down to a few micrometres in diameter may be seen under high magnification
- The lower limit is reached when the particle size approaches the wavelength of visible light, 0.4–0.7 µm
- For submicron-sized particles, it is essential to use **electron microscopy**
  - Features as small as a few Å across can be imaged readily

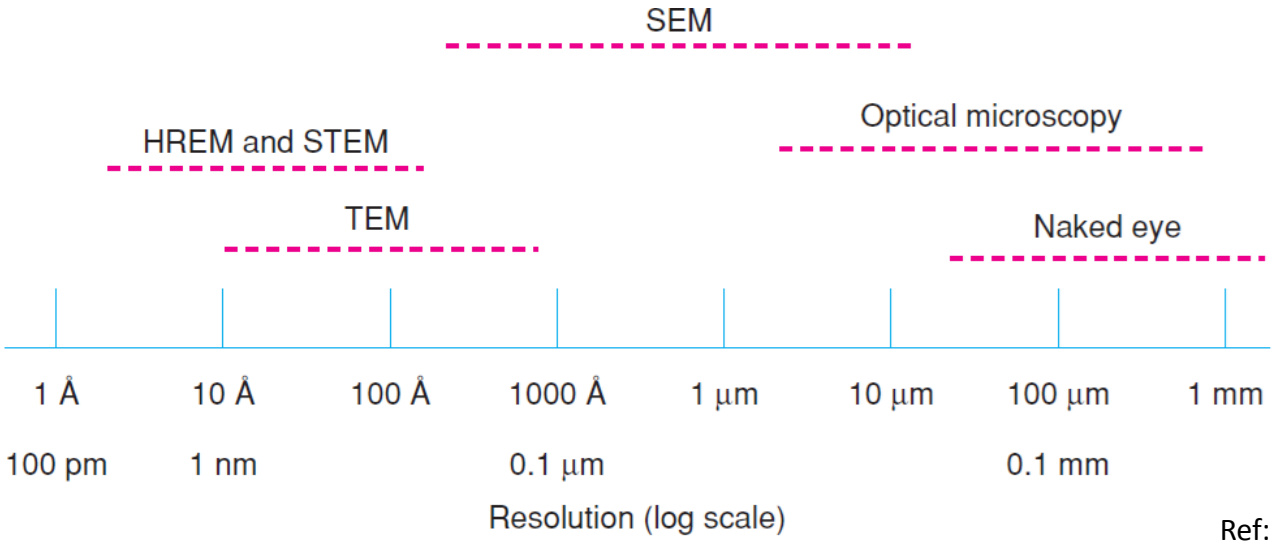

Ref: West p. 331

Figure 6.4 Working ranges of various techniques used for viewing solids. TEM = transmission electron microscopy; HREM = high-resolution electron microscopy; SEM = scanning electron microscopy.

Scanning Electron Microscopy

See [Solid State Chemistry Wiki]

- In SEM, electrons from the electron gun, accelerated through 5–50 keV, are focused to a small spot, 50–500 Å in diameter, on the sample surface
- Usually detection of **secondary electrons**
- The main application of SEM is for surveying materials under high magnification and providing information on sizes, shapes and compositions as seen from solid surfaces

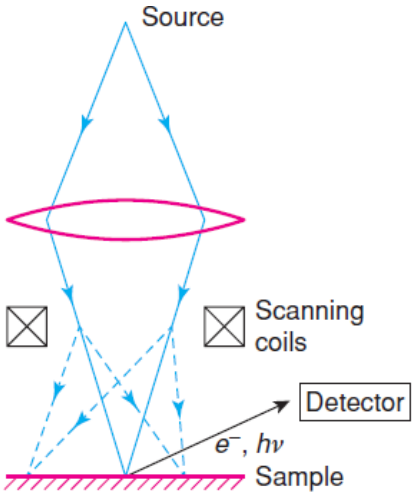

Figure 6.8 *Principle of the scanning electron microscope.*

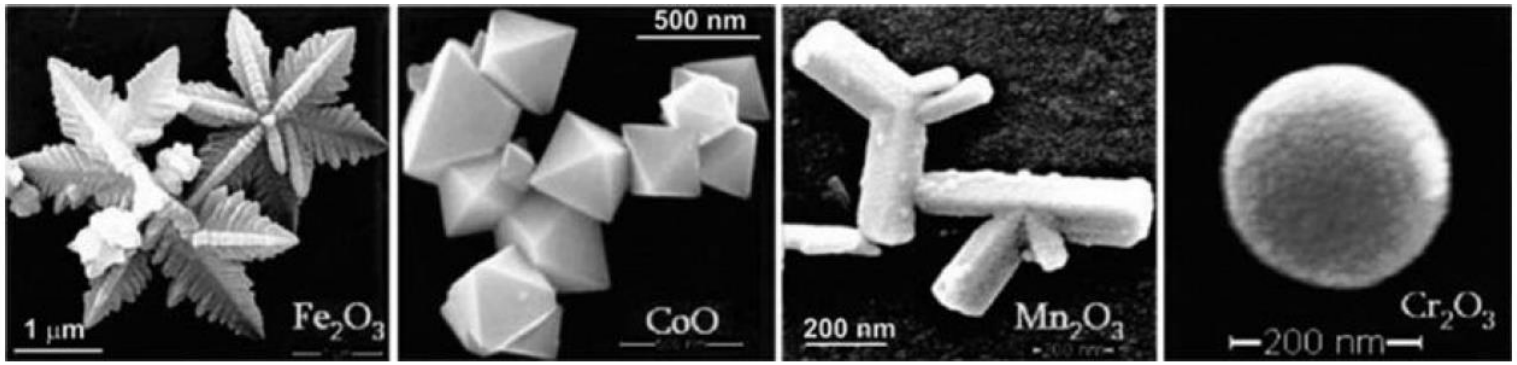

Figure 4.9 *SEM images of various metal oxide nanostructures. Reproduced with permission from I. Bilecka and M. Niederberger,* Nanoscale, *2, 1358, © 2010 Royal Society of Chemistry.*

Ref: West p. 204, 281

Transmission Electron Microscopy

See Solid State Chemistry Wiki

- TEM detects **transmitted** electrons and radiation (SEM is based on **reflection**)
- Nowadays enables even atomic resolution (≤ 1 Å)
- With TEM, both **electron diffraction patterns** and **magnified images** can be obtained from the same sample area
  - Electron diffraction patterns give unit cell and space group information
  - In imaging mode, TEM gives morphological information on the sample
- The first TEM was in fact built by Max Knoll and Ernst Ruska in 1931 (Nobel 1986)

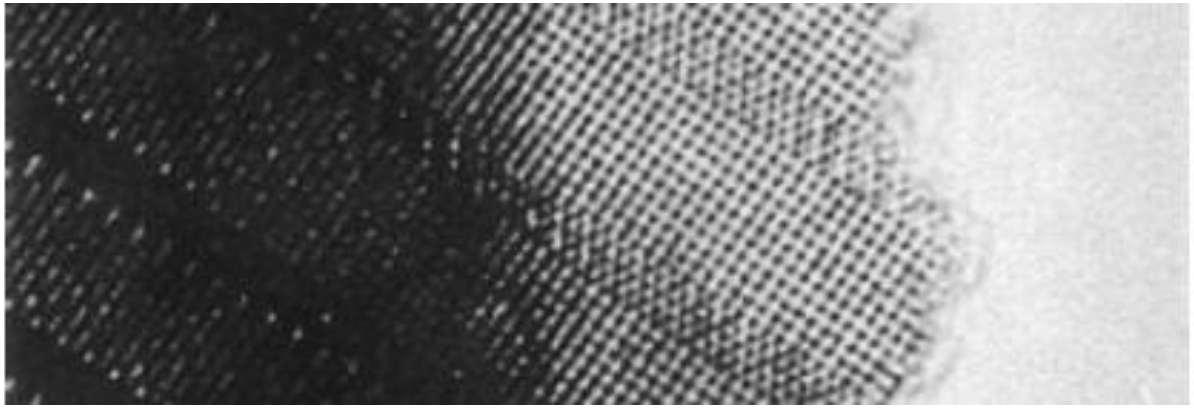

Figure 6.14 *High-resolution electron micrograph of an intergrowth tungsten bronze, $Rb_{0.1}WO_3$. Black dots represent WO_6 octahedra. The structure may be regarded as an intergrowth of primitive cubic WO_3 (strips of black dots based on a square grid) and hexagonal WO_3 containing Rb (narrow strips of black dots on a hexagonal grid). Photograph courtesy of Dr M. Sundberg, University of Stockholm, Department of Chemistry.*

Ref: West p. 288

TEM (2)

- TEM resolution has been pushed to the sub-ångström level with sophisticated ***aberration correction*** techniques
- Important limitation: Extensive sample preparation is required to produce a sample thin enough to be electron transparent
- The structure of the sample may change during the preparation process
- The field of view is relatively small, so the analyzed region may not represent the whole sample.
- The sample may be damaged by the electron beam, particularly in the case of biological materials (lower operation voltage helps)

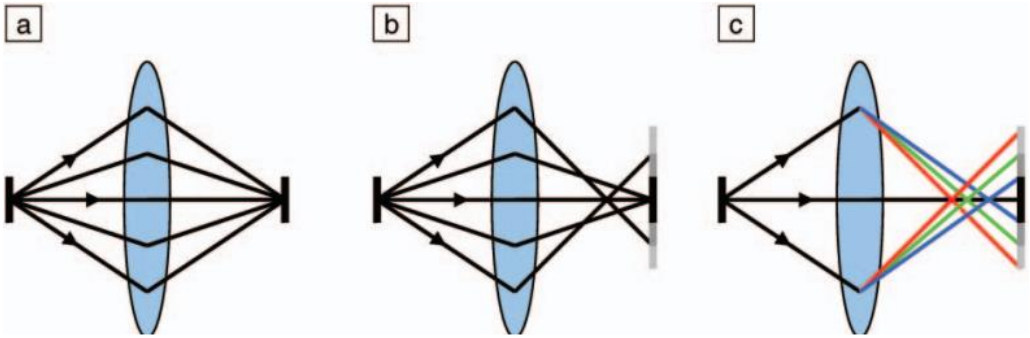

Figure 2. Illustration of certain lens aberrations. (a) A perfect lens focuses a point source to a single image point. (b) Spherical aberration causes rays at higher angles to be overfocused. (c) Chromatic aberration causes rays at different energies (indicated by color) to be focused differently. **MRS BULLETIN • VOLUME 31 • JANUARY 2006**

Optical, transmission (TEM) and aberration-corrected electron microscopes (ACTEM)

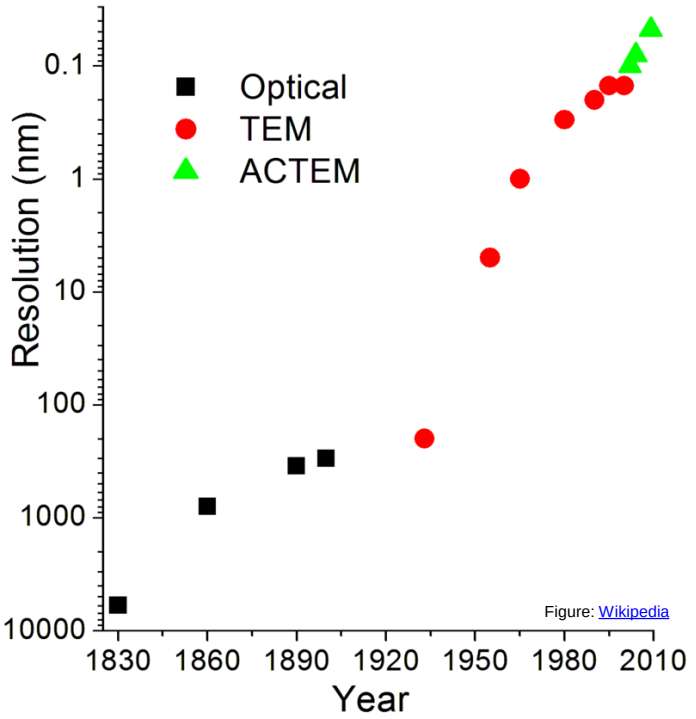

Sub-Ångström TEM

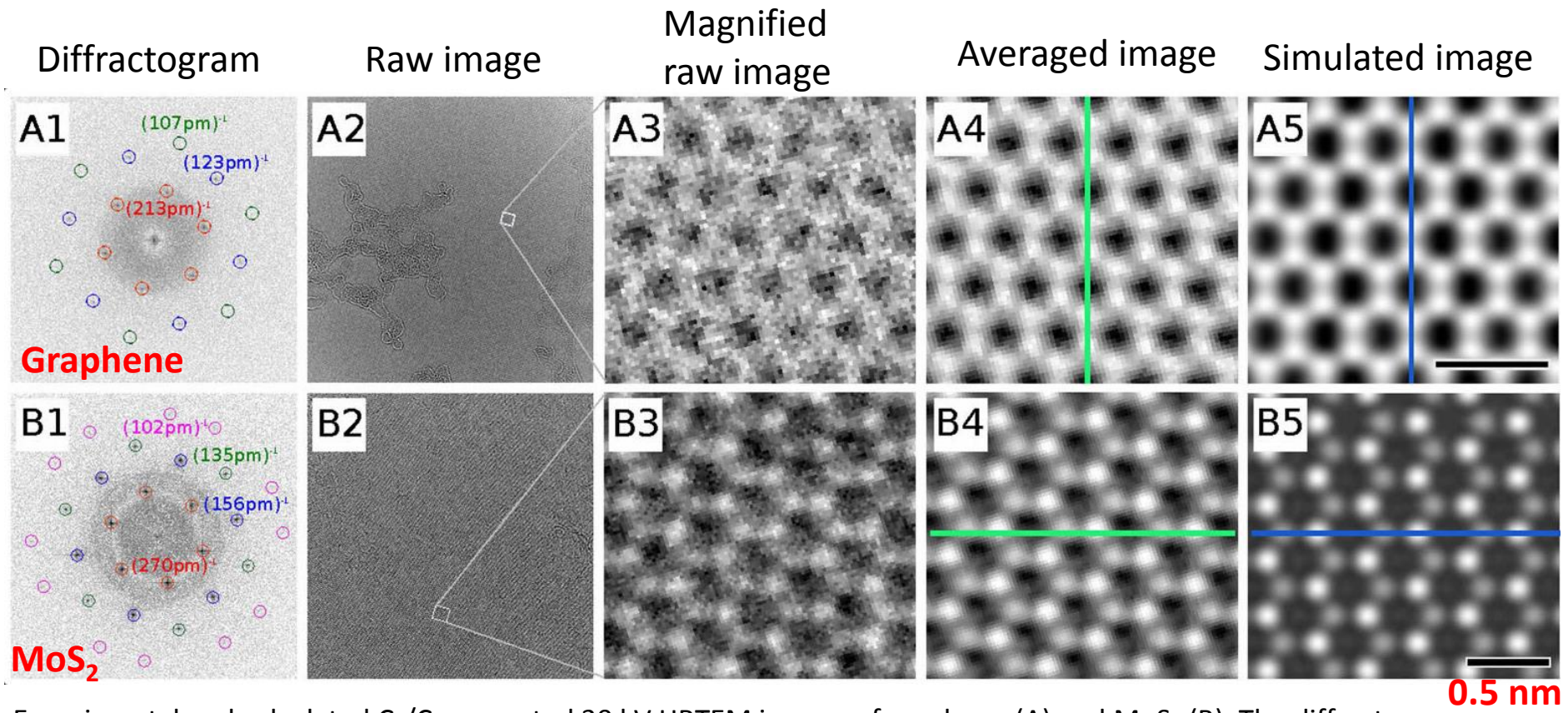

Experimental and calculated C_S/C_C-corrected 30 kV HRTEM images of graphene (A) and MoS_2 (B). The diffractograms (A_1 and B_1) of the experimental raw images of graphene (A_2) and MoS_2 (B_2) in bright-atom contrast (field of view 40 x 40 nm^2) indicate the achieved resolution. The magnified raw images (A_3 and B_3) directly allow for identifying the atomic structure. The averaged experimental images (A_4 and B_4) show a strong signal-to-noise improvement and are in good agreement with the simulated images (A_5 and B_5). The scale bars in A_5 and B_5 correspond to 0.5 nm

http://www.salve-project.de/newspress/SALVE-CC-correction-realized.html

Structural challenge: *m-allo*-Ge

Bulk Synthesis and Structure of a Microcrystalline Allotrope of Germanium (*m-allo*-Ge)

Florian Kiefer,[†] Antti J. Karttunen,[‡] Markus Döblinger,[§] and Thomas F. Fässler*[,†]

Chemistry of Materials, **2011**, *23*, 4578–4586.

ABSTRACT: An easy to reproduce and scale-up method for the preparation of a microcrystalline allotrope of germanium is presented. Based on the report of the oxidation of a single crystal of Li_7Ge_{12} the synthesis and structure determination of a powdered sample of Li_7Ge_{12} is investigated. Besides the known oxidation of Li_7Ge_{12} with benzophenone a variety of protic solvents such as alcohols and water were used as oxidants. Electron energy loss spectroscopy (EELS) proves that the reaction products do not contain Li. The structure determination of the powder samples based on selected area electron diffraction (SAED), powder X-ray diffraction, quantum chemical calculations (DFT-B3LYP level of theory), and simulated powder X-ray diffraction diagrams obtained using the DIFFaX and FAULTS software packages show that the microcrystalline powders do not match any of the existing structures of germanium including the rough model of so-called *allo*-Ge. It is shown that the structural motif of layered Ge slabs of the precursor Li_7Ge_{12} that contain five-membered rings is retained in microcrystalline *allo*-Ge (*m-allo*-Ge). The covalent connectivity between the slabs and the statistic of the layer sequence is determined. According to B3LYP-DFT calculations of a periodic approximate model a direct band gap is expected for *m-allo*-Ge.

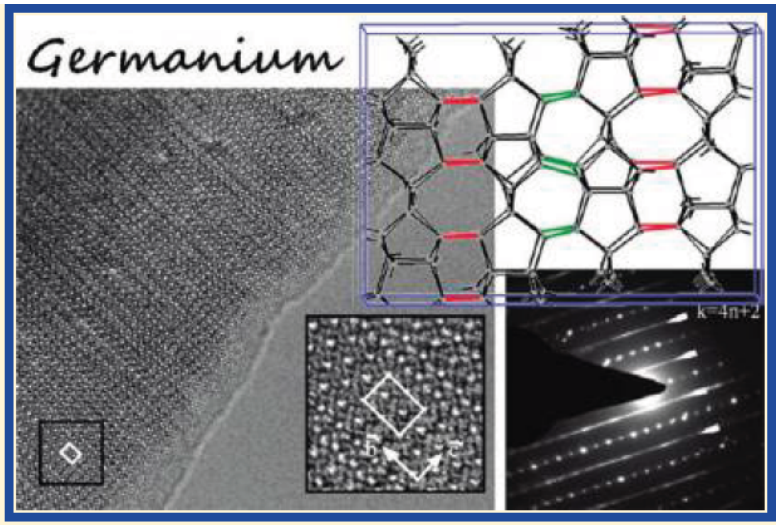

From Li_7Ge_{12} to *m-allo*-Ge (1)

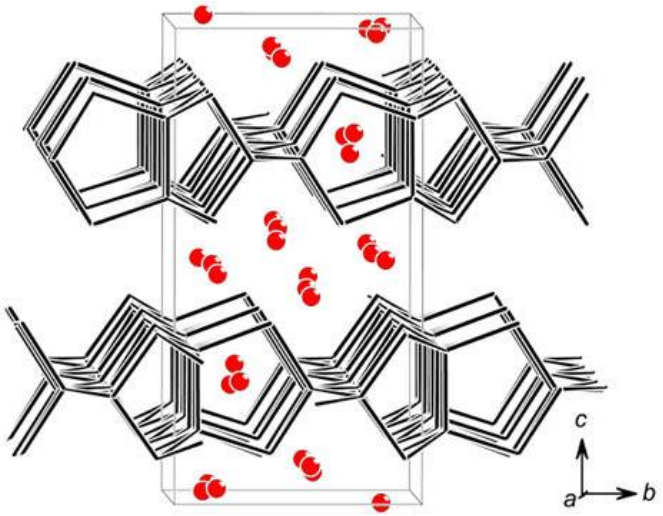

Li_7Ge_{12} precursor (*P*2/*n*)

H_2O / EtOH

Removal of Li
(de-intercalation)

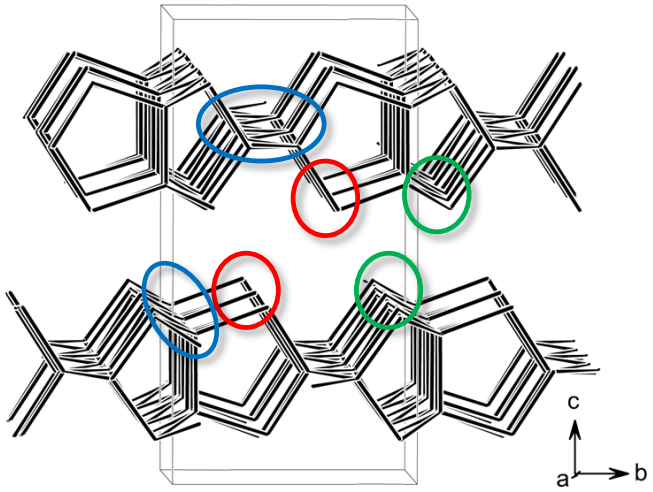

Ge atoms with **two**, **three** or **four** bonds

Oxidative coupling of the layers

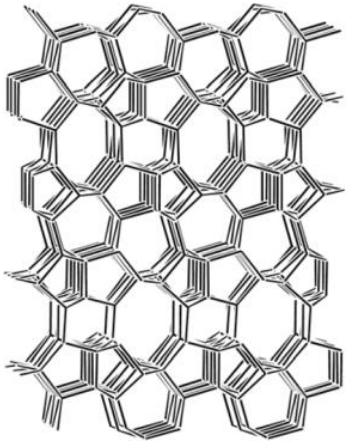

***m-allo*-Ge**

HRTEM for *m-allo*-Ge:

Stacking faults along *c*-axis

Li_7Ge_{12} precursor (*P*2/*n*)

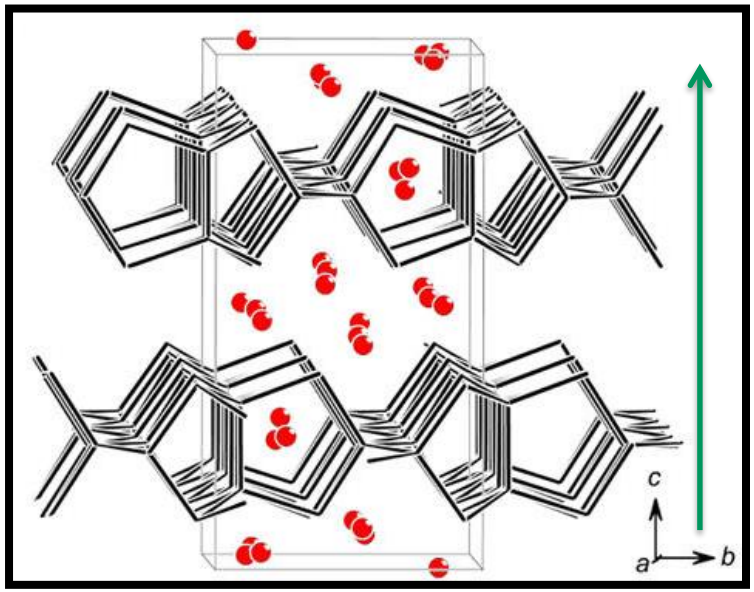

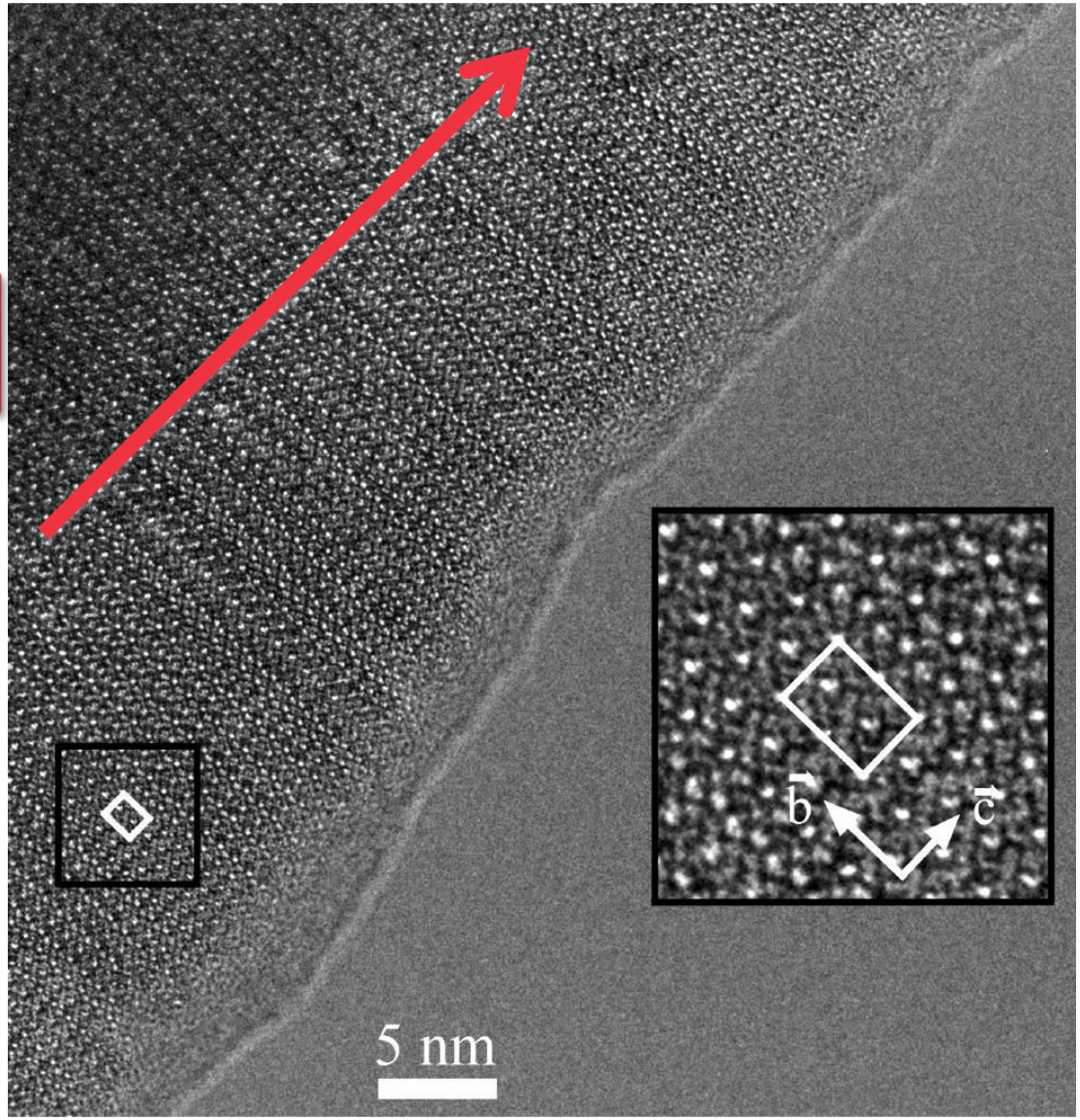

Figure 4. HRTEM image of *m-allo*-Ge recorded along [100]. While being perfectly periodic along *b*, the image reveals considerable disorder along *c*. The area outlined by a black box is enlarged on the right side of the figure. The white box indicates the projected unit cell.

Statistical model for the stacking faults

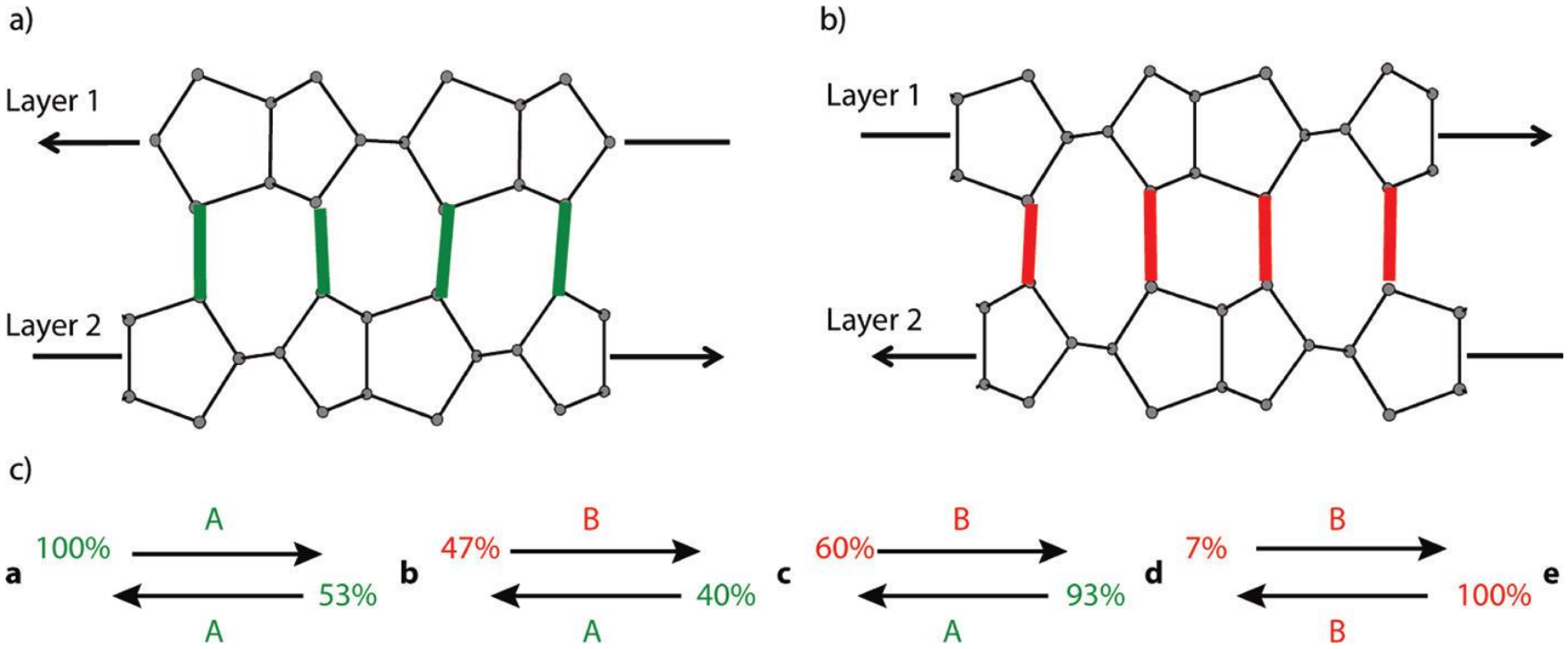

Figure 7. The structural model **6** of *allo*-Ge with stacking faults based of a statistical sequence of a) interlayer connection **A** including 7-membered rings and b) interlayer connection **B** including 6- and 8-membered rings. c) Transition probability of the occurrence of the interlayer connection type **A** and **B**. Layers (a, c, e) and (b, d) in Figure 7c correspond to the layer types 1 and 2 in Figure 7a-b, respectively. See text for more details.

The model derived from quantum chemical calculations was refined with ***FAULTS*** program package to match the experimental powder pattern (~Rietveld refinement)

Total probabilities of interlayer bonding types: A: 60%, B: 40%

Powder XRD for the structural model

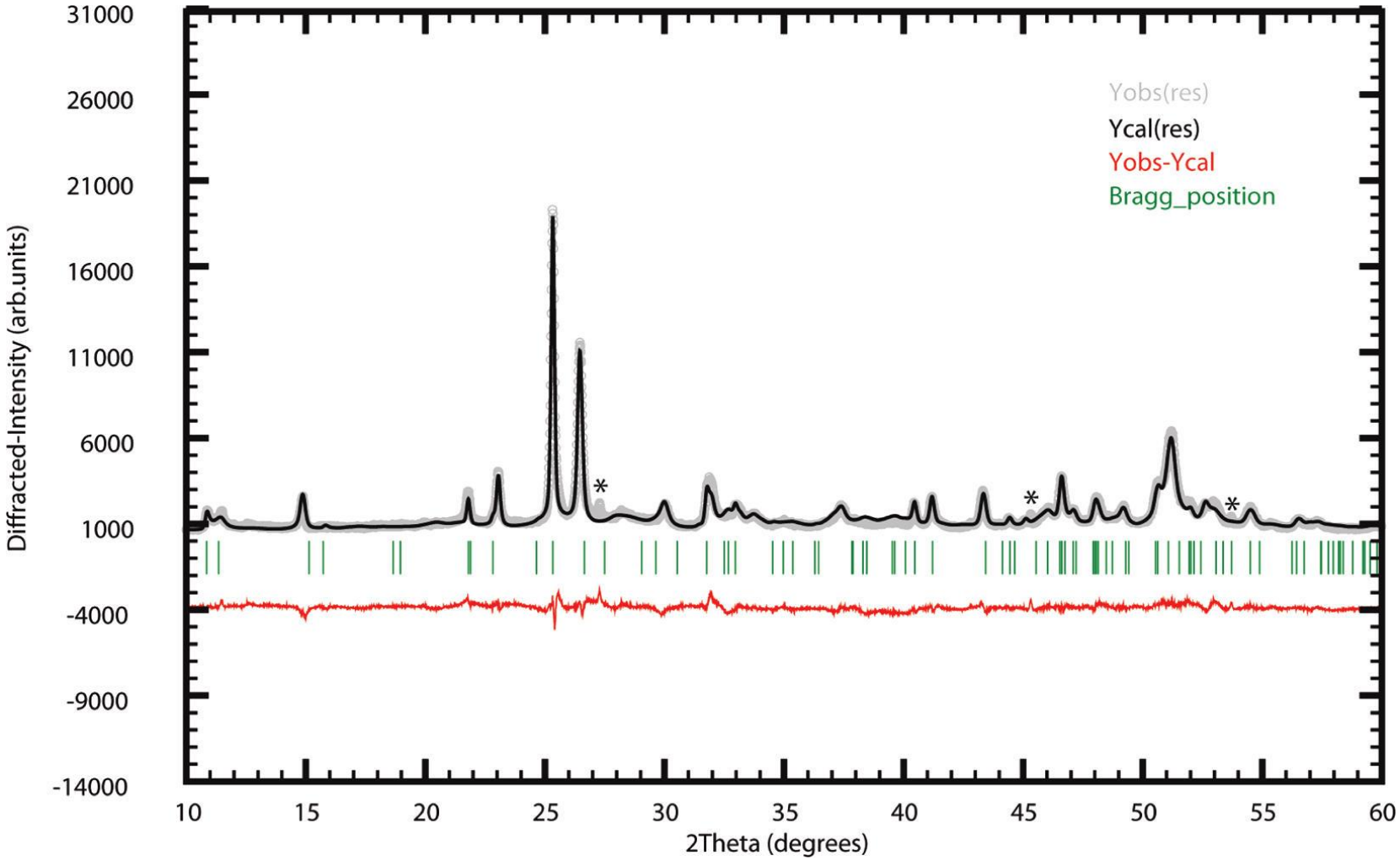

Figure 8. Powder X-ray diffractogram of the *m-allo*-Ge. Experimental data are shown as a gray line; reflections based on structural model **6** with stacking faults along the *c* axis are simulated with the FAULTS software and shown as a black line. The difference diagram is shown in red. Reflections denoted with (*) originate from α-Ge.

Electron Diffraction for *m-allo*-Ge

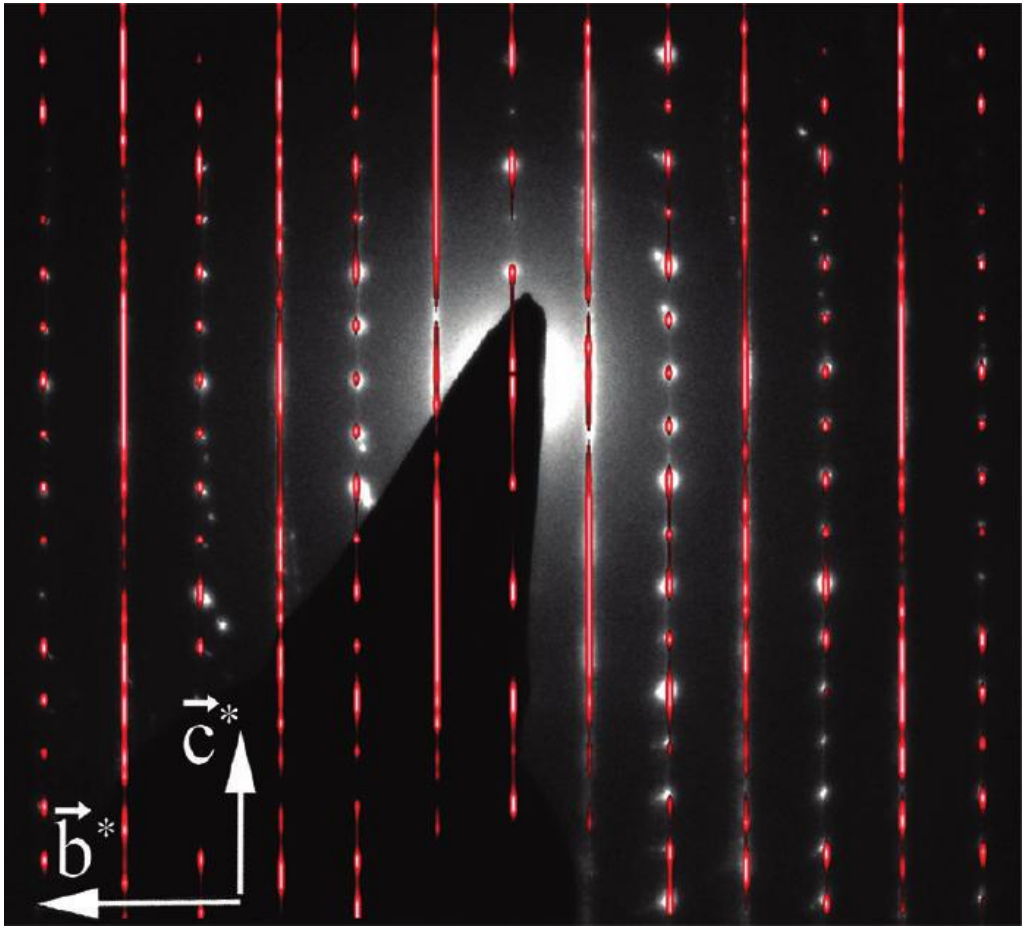

Figure 9. Simulated electron diffraction pattern for the *allo*-Ge model **6** (red) superimposed on an experimental electron diffraction pattern of *m-allo*-Ge (reciprocal *0kl* layer, cf. Figure 3b).